Advanced and Sustainable Technologies
ASET
E-ISSN 2976-2294
Volume 5, No 2, September 2026 [331-338]

Impedance Study of a NiO-BCZY|BCZY|LSCF Single Cell With and Without Anode Reforming Layer

Nurul Hazwani Yusof[1], Suhaida Dila Safian[1,3], Abul Kalam Azad[2], Lidyayatty Abdul Malik[3,4], Abdul Mutalib Md Jani[3,4] and Nafisah Osman[1,3]*

[1]Faculty of Applied Sciences, Universiti Teknologi MARA, 02600 Arau, Perlis, Malaysia.
[2]Faculty of Integrated Technologies, Universiti Brunei Darussalam, Jalan Tungku Link, Gadong, BE 1410, Brunei Darussalam.
[3]Proton Ceramic Fuel Cells Research Group, Faculty of Applied Sciences, Universiti Teknologi MARA, 40450 Shah Alam, Malaysia.
[4]Faculty of Applied Sciences, Universiti Teknologi MARA, 35400 Tapah Road, Tapah, Perak, Malaysia.

Received 28 May 2026, Revised 30 June 2026, Accepted 21 July 2026

ABSTRACT

Proton ceramic fuel cells (PCFCs) have attracted considerable attention due to their potential for fuel flexibility with hydrocarbons and syngas, making them promising candidates for next-generation energy conversion systems that support Sustainable Development Goals (SDGs) 7 and 9. Although anode reforming layers (ARLs) have been investigated to improve hydrocarbon operation, their influence on the intrinsic electrochemical processes at the triple-phase boundary (TPB) remains insufficiently understood. This study addresses this gap by investigating the electrochemical behaviour of a 50 wt% CeO_2–50 wt% BaO ARL using electrochemical impedance spectroscopy (EIS) and distribution of relaxation times (DRT) analysis. An anode-supported cell with the configuration NiO-BCZY|BCZY|LSCF (BCZY = $BaCe_{0.54}Zr_{0.36}Y_{0.1}O_{2.95}$; LSCF = $La_{0.6}Sr_{0.4}Co_{0.2}Fe_{0.8}O_{3-\delta}$); with ARL (Cell 1) and without ARL (Cell 2) was evaluated under humidified 10% H_2–90% N_2 atmosphere at 700°C. The Nyquist plots showed that Cell 1 exhibited lower polarization resistance than Cell 2, indicating enhanced overall electrode kinetics. Further DRT analysis revealed that the most pronounced reduction occurred in the high-frequency process (P1), followed by a smaller reduction in the intermediate-frequency process (P2), suggesting improved interfacial charge-transfer kinetics at the TPB. These findings provide mechanistic insight into the role of the CeO_2–BaO ARL and establish a basis for its future application under hydrocarbon fuels.

Keywords: Anode Reforming Layer, Nyquist Plot, Relaxation times (τ).

1. INTRODUCTION

Proton Ceramic Fuel Cells (PCFCs) represent a transformative technology in the field of clean energy conversion, operating at intermediate temperatures of 500–800 °C. This clean energy conversion produces fewer emissions and converts energy more efficiently than traditional combustion engines, such as those powered by fossil fuels [1]. Aside from that, PCFCs offer significant advantages over traditional solid oxide fuel cells (SOFCs) and, unlike SOFCs, conduct protons through ceramic electrolytes and can utilize hydrocarbon fuels [2, 3]. These features position PCFCs as promising candidates for stationary power generation and green hydrogen production, with the flexibility to use hydrogen and hydrocarbon gases, aligning with the United Nations Sustainable Development Goals (SDGs) 7 and 9 [4–6].

*Corresponding author: fisha@uitm.edu.my

While these advantages are significant, they also come with certain drawbacks. The electrochemical performance of PCFCs is strongly influenced by the types of fuels. At the anode side, different fuels will affect the oxidation and charge transfer processes where the reactions occur at the triple phase boundary (TPB) [7]. For hydrogen fuel, the oxidation reaction is more straightforward than that of hydrocarbon fuel [8, 9]. Thus, the incorporation of the anode reforming layer (ARL) has been studied to enhance cell robustness and improve fuel reforming capability. Although ARL has been widely investigated to improve the hydrocarbon tolerance and catalytic performance of proton ceramic fuel cells (PCFCs), most studies have focused primarily on overall cell performance with hydrocarbon fuels. In contrast, the intrinsic electrochemical processes and reaction kinetics associated with ARL incorporation during hydrogen operation remain poorly understood, particularly at the triple-phase boundary (TPB). Since hydrogen provides a well-defined electrochemical environment without the complexity of hydrocarbon reforming reactions, investigating the ARL under hydrogen conditions enables the individual kinetic processes to be distinguished before extending the study to hydrocarbon fuels [10,11].

Therefore, this study investigates the impedance characteristics of an anode-supported NiO-BCZY|BCZY|LSCF cell with and without ARL in a wet hydrogen atmosphere over the temperature range of 500–800 °C. The novelty of this study lies in the combined application of electrochemical impedance spectroscopy (EIS), equivalent-circuit fitting, and distribution of relaxation times (DRT) analysis to distinguish the individual electrochemical processes influenced by the ARL. This approach enables identification of the dominant kinetic processes and charge-transport behavior at the triple-phase boundary (TPB), thereby establishing a mechanistic understanding of the ARL prior to methane (CH_4) exposure.

2. MATERIAL AND METHODS

2.1 Powder synthesis

The NiO-BCZY (BCZY = $BaCe_{0.54}Zr_{0.36}Y_{0.1}O_{2.95}$) anode composite powder containing 50 wt.% NiO and 50 wt.% BCZY was synthesized via citrate complexation. Stoichiometric amounts of nickel, barium, cerium, zirconium, and yttrium nitrate precursors were dissolved in 150 mL of deionized water and mixed with citric acid under continuous stirring overnight to form a metal-citrate complex. The solution pH was adjusted to 6.9 ± 0.5 with concentrated ammonia, and the mixture was stirred overnight. Subsequently, the solution was heated at 120°C to form a viscous black gel and dried at 325°C. The dried precursor was pre-calcined at 325°C for 2 h and then calcined at 1100°C for 6 h, with a heating/cooling rate of 10°C min^{-1} to obtain NiO-BCZY powder [3]. As for electrolyte, the BCZY powder was synthesized via a modified citrate–EDTA complexation route using the sol-gel method. Stoichiometric amounts of barium, cerium, zirconium, and yttrium nitrate precursors were dissolved in 150 mL of deionized water under magnetic stirring until complete dissolution. Citric acid (CA) was subsequently added, and the mixture was stirred overnight to form a metal-citrate complex solution (Beaker A). Separately, EDTA was dissolved in 200 mL of ammonia solution under continuous stirring (Beaker B). The EDTA solution was slowly introduced into Beaker A and stirred overnight, then ethylene glycol was added as a polymerizing agent, and the mixture was stirred further. The pH of the solution was adjusted to 7.0 ± 0.5 using concentrated ammonia. The resulting solution was heated at 120°C to remove excess water, forming a viscous black gel, which was then dried at 325°C to obtain a hardened gel. The dried precursor was pre-calcined at 325°C for 2 h and subsequently calcined at 1050°C for 11 h with a heating/cooling rate of 10°C min^{-1} to obtain fine BCZY powder [12].

For the cathode powder, the $La_{0.6}Sr_{0.4}Co_{0.2}Fe_{0.8}O_{3-\delta}$ (LSCF) powder was prepared using the citrate–EDTA method. Stoichiometric quantities of lanthanum, strontium, cobalt, and iron nitrate precursors were dissolved in 100 mL of deionized water and mixed with CA and EDTA at a molar

ratio of 1:2:1. After complete dissolution of EDTA, ethylene glycol was added, and the solution was gradually heated to form a viscous gel. The gel was dried at 150°C for 15 h in a Venticell oven and calcined at 900°C for 4 h with a heating/cooling rate of 10°C min^{-1} to produce LSCF powder [13]. Lastly, the catalyst powders, BaO and CeO_2, were synthesized separately as previously reported [14]. Barium nitrate and cerium nitrate precursors were individually dissolved in 50 mL of deionized water to form solutions C and D, respectively, while citric acid monohydrate dissolved in 50 mL of deionized water formed solution E. Solution E was mixed separately with solutions C and D and stirred for 2 h. Each mixture was heated to 80°C to form a homogeneous gel and dried at 85°C in a Venticell oven. The dried powders were ground and subjected to two-step calcination. For BaO, the precursor was calcined at 450°C for 2 h, then at 800°C for 4 h, with a heating rate of 2°C min^{-1}. For CeO_2, the precursor was first calcined at 300°C for 2 h at a heating rate of 1°C min^{-1}, then calcined at 450°C for 4 h at a heating rate of 2°C min^{-1}. Then, the obtained powders, CeO2 and BaO, were mixed into 20ml of ethanol using a mortar and pestle at a ratio of 50 wt% each.

2.2 Fabrication of a Single Cell

An anode-supported button-type proton-conducting fuel cell (PCFC) was fabricated via a combination of dry pressing and spin-coating techniques, as done in the previous work [7]. However, the fabrication of ARL involved preparing a catalyst slurry. A 6 wt.% ethyl cellulose (EC) binder was thoroughly stirred with 94 wt.% terpineol to form a binder solution. 50wt%CeO_2 – 50wt%BaO powders were weighed and mixed with the binder solution at a ratio of 1:1 (powder: binder solution). The mixtures were stirred for 30 min, sonicated for 1 h, and stirred again for 30 min to ensure uniform dispersion. The resulting slurries were spin-coated onto sintered NiO-BCZY anode substrate pellets. The single cell with ARL was named Cell 1, and the one without ARL was named Cell 2.

2.3 Characterization and Electrochemical Measurement

The electrochemical performance of Cell 1 and Cell 2 was evaluated using an in-house electrochemical impedance spectroscopy (EIS) system. Before testing, the pellets were coated with Pt paste on both sides and then heat-treated at 900°C for 1 h at a heating/cooling rate of 10°C min^{-1}. The pellets were subsequently mounted onto a sample holder using a non-conductive ceramic sealant (Ceramabond™ 571, Aremco), dried overnight, and further dried at 90°C and 250°C for 2 h each in a Venticell oven.

The mounted sample was inserted into a conductivity cell tube and placed inside a furnace for EIS measurements. Before testing, the Cell 1 and Cell 2 were reduced and stabilized at 700°C for 5 h under a humidified 10% H_2–90% N_2 atmosphere. Impedance measurements were then performed at 700 °C over a frequency range of 1 Hz–1 MHz. [15]. This temperature was selected as the representative operating condition for detailed Nyquist and DRT analyses. The impedance spectra were acquired using a ZIVE SP2 electrochemical workstation (WonATech) controlled by a personal computer, and the resulting data were analyzed and replotted using OriginLab software. The relaxation times (τ) were calculated using DRT self-software packages self-software packages generated in MATLAB code, and the DRTtools parameters were kept constant throughout the analysis [7,13].

3. RESULTS AND DISCUSSION

Figure 1 presents the Nyquist plot of Cell 1 and Cell 2 measured at 700 °C under humidified H_2. The equivalent circuit model, Rs-R1|Q1-R2|Q2-R3|Q3, adequately describes the impedance behaviour and separates the contribution from high to low-frequency processes [16]. Both cells exhibit depressed semicircles, indicating the presence of an impedance pattern, with multiple

electrochemical processes contributing simultaneously to the overall polarization resistance [16]. However, unlike the typical impedance pattern of the anode-supported single cell as reported by Senari et al. [17], the spectra do not originate from the zero-impedance point due to the inherent ohmic resistance of the cell, which may arise from the electrolyte, grain boundaries, electrode contacts, and current-collector contacts.

Cell 1 showed a considerably smaller semicircle and lower total impedance compared to Cell 2, indicating the improvement of electrochemical activity. Equivalent-circuit fitting revealed that the ohmic resistance (Rs) decreased slightly from 5.89 $\Omega \cdot cm^2$ for Cell 2 to 5.24 $\Omega \cdot cm^2$ for Cell 1. Since Rs represents the combined ohmic contributions from the electrolyte, electrical contacts, and current collectors, the small reduction suggests that incorporating the 50 wt% CeO2–50 wt% BaO anode reforming layer (ARL) does not introduce additional ohmic losses and may slightly improve interfacial contact. More importantly, the fitting confirmed that the performance enhancement was primarily associated with reductions in the polarization resistance (Rp). The R_p decreased from 80.52 $\Omega \cdot cm^2$ (Cell 2) to 28.26 $\Omega \cdot cm^2$ (Cell 1), corresponding to ~65% reduction. Moreover, from the fitted parameter analyses, the most significant values occur in the low-frequency region (R3), as R_3 decreases from 54.54 $\Omega \cdot cm^2$ (Cell 2) to 5.32 $\Omega \cdot cm^2$ (Cell 1). According to Karmakar [18], the low-frequency response in the electrochemical systems is generally associated with adsorption, diffusion and mass-transfer phenomena. Therefore, this substantial reduction in R_3 of Cell 1 compared to Cell 2 indicated that the CeO_2–BaO, as an ARL, effectively suppresses polarization-associated effects and facilitates surface reactions at the anode. This may be due to the catalytic characteristics of CeO2, which possess abundant oxygen vacancies and reversible Ce4+/Ce3+ redox couples, providing active sites for catalytic reactions and promoting reactant activation, as reported by Wang et al. [19]. In the present work, the incorporation of CeO_2 together with BaO is suggested to enhance the electrochemical activity at the TPB, possibly by facilitating H_2 adsorption and dissociation and increasing the availability of catalytically active reaction sites. This interpretation is supported by the observed reductions in R_p and DRT peak intensities, although direct morphological evidence of the ARL/anode interface is beyond the scope of the present study.

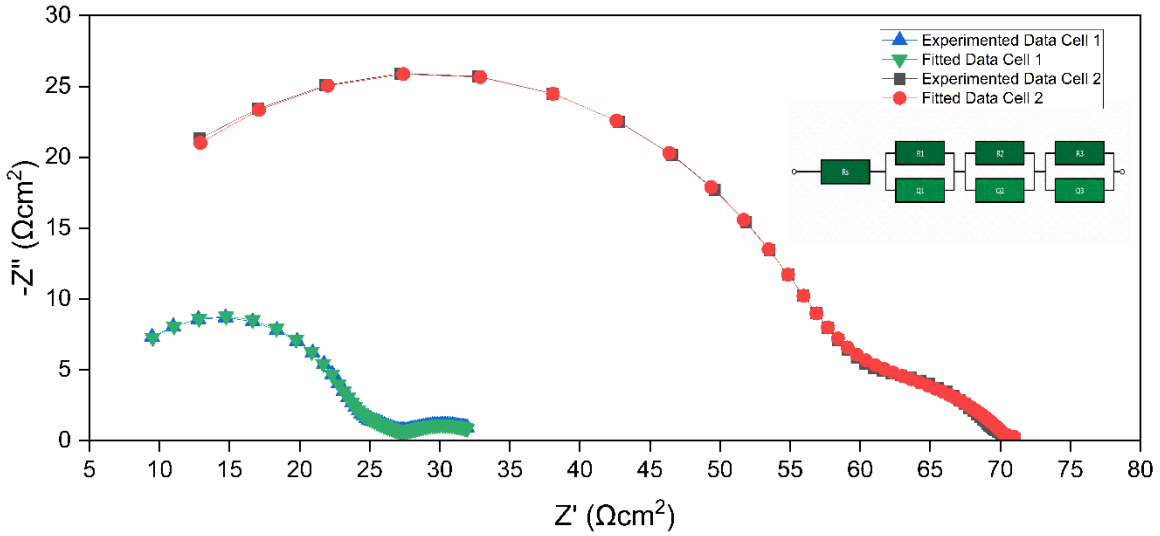

Figure 1: The Impedance spectrum of Cell 1 and Cell 2 under humidified H_2 at 700 °C.

Other than that, the high-frequency resistance (R_1) decreased from 16.13 $\Omega \cdot cm^2$ (Cell 2) to 6.37 $\Omega \cdot cm^2$ (Cell 1), indicating that the interfacial charge-transfer kinetics had been improved with the presence of the ARL. As reported by Tsvetkov et al [20], the electrochemical performance of PCFCs is strongly influenced by their interface characteristics and TPB engineering. Hence, the reduction in R_1 observed in Cell 1 suggests that the CeO_2–BaO layer may contribute to the

extension of the electrochemically active regions, and that proton transfer has been facilitated across the electrode/electrolyte interface.

Consequently, the Distribution of Relaxation Times (DRT) analysis was performed to further distinguish the individual kinetic processes responsible for the observed reduction in polarization resistance based on their relaxation time (τ) [7,13,16]. The DRT analysis successfully resolved the impedance response into five relaxation processes (P1–P5). As shown in Figure 2, five relaxation processes (P1 – P5) were identified for both cells within the τ range of 10^{-6} – 10 s. Both cells appear to follow a similar electrochemical reaction pathway, as indicated by the similar peak positions observed, even in the presence of ARL in Cell 1. However, the differences in the peak intensity between the two cells reflect changes in the resistance associated with each kinetic process. Compared with Cell 2, Cell 1 exhibits lower DRT peak intensities for P1 and P2, indicating that the CeO_2–BaO (ARL) effectively reduces the resistance associated with the dominant and intermediate electrochemical kinetic processes. The reduction in P1 is consistent with the smaller high-frequency impedance response observed in the Nyquist plot. It is commonly associated with improved interfacial charge-transfer kinetics. In contrast, the reduction in P2 suggests enhanced hydrogen oxidation kinetics at the TPBs [7,13,16]. In contrast, only minor differences are observed in P3-P5 between Cell 1 and Cell 2, suggesting that slower reaction processes contribute less to the overall improvement in electrochemical performance. The DRT results indicate that the enhancement in electrochemical performance is primarily attributed to the reduction in the dominant and intermediate kinetic resistances, as evidenced by the lower P1 and P2 peak intensities. Furthermore, the similar relaxation times observed for both cells suggest that incorporating the CeO_2–BaO ARL does not substantially alter intrinsic electrochemical processes but instead reduces the resistance associated with existing reaction pathways, thereby promoting more efficient hydrogen oxidation kinetics [19,21,22].

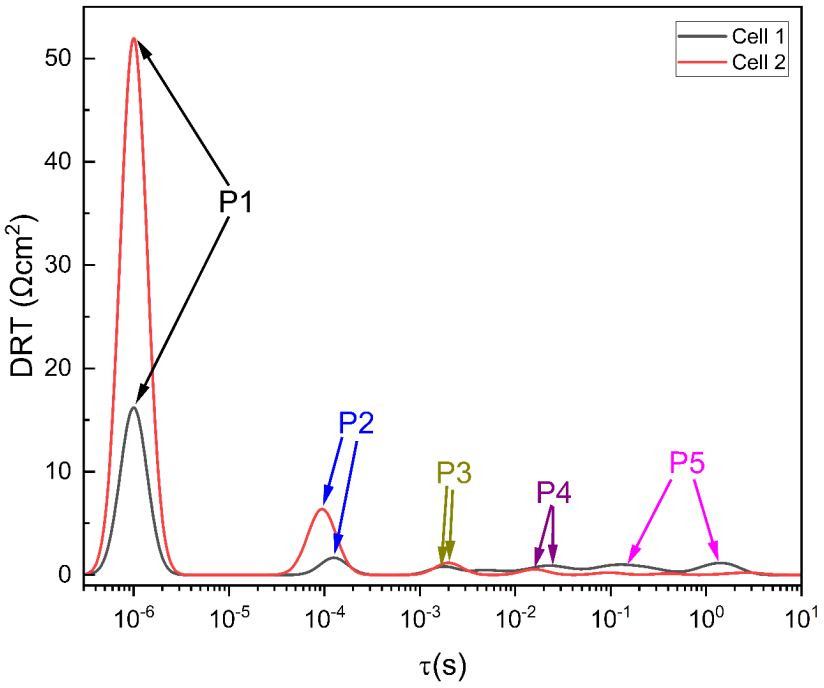

Figure 2: The DRT Analysis of Cell 1 and Cell 2 under humidified H_2 at 700 °C.

These findings are in good agreement with the Nyquist analysis, in which the ARL-modified cell exhibited a smaller impedance semicircle and lower polarization resistance, confirming that the improved electrochemical performance primarily stems from reduced dominant kinetic resistances while maintaining the same electrochemical processes. It should be noted that the

equivalent-circuit fitting and DRT analyses provide complementary interpretations of the impedance response. While the equivalent-circuit fitting showed the largest reduction in the low-frequency resistance component (R_3), the DRT analysis revealed the most pronounced reduction in the high-frequency process (P_1). This difference reflects the distinct analytical principles of the two methods, whereby equivalent-circuit fitting quantifies the resistance of predefined electrical elements, whereas DRT resolves the impedance spectrum into relaxation-time distributions associated with individual electrochemical processes. Nevertheless, both analyses consistently demonstrate that incorporating the CeO_2–BaO ARL effectively reduces overall polarization resistance and enhances electrode kinetics.

4. CONCLUSION

The incorporation of the 50wt%CeO_2 – 50wt%BaO as an anode reforming layer (ARL) significantly improved the electrochemical performance of the NiO-BCZY|BCZY|LSCF single cell at 700°C. The Nyquist analysis demonstrated a substantial reduction in the overall R_p, indicating that the enhanced electrode kinetics and reduced electrochemical losses after the incorporation of ARL. The ARL-modified cell showed lower resistance contributions for the dominant relaxation processes (P1 and P2), indicating that the CeO_2–BaO ARL enhances the existing electrochemical kinetics. Overall, the combined Nyquist and DRT analyses demonstrate that the CeO_2–BaO ARL enhances the electrochemical activity of the anode by reducing the dominant kinetic resistances in a hydrogen-containing atmosphere. These findings provide a fundamental electrochemical baseline for evaluating the influence of the ARL during subsequent operation under CH_4, where methane reforming and carbon deposition are expected to affect the cell's electrochemical behaviour.

ACKNOWLEDGEMENTS

The authors thank the Ministry of Higher Education, Malaysia, for the Fundamental Research Grant Scheme (FRGS/1/2024/STG05/UiTM/01/1) and Universiti Teknologi MARA for the support and facilities.

REFERENCES

[1] Basbus, J. F., Arce, M. D., Napolitano, F. R., Troiani, H. E., Alonso, J. A., Saleta, M. E., Mogni, L. V. Revisiting the crystal structure of BaCe0. 4Zr0. 4Y0. 2O3− δ proton conducting perovskite and its correlation with transport properties. ACS Applied Energy Materials, vol 3, issue 3 (2020) pp.2881-2892. https://doi.org/10.1021/acsaem.9b02498

[2] Affandi, N. S. M., Malik, L. A., Safian, S. D., Othman, M. H. D., Osman, N. Proton conduction in perovskite solid electrolyte for proton ceramic fuel cell application at intermediate temperatures: A short review. Jurnal Kejuruteraan, vol 35, issue 1 (2023) pp.59-63. https://doi.org/10.17576/jkukm-2023-35(1)-06

[3] Malik, L. A., Rosdi, M. N. N. M., Hassan, O. H., Jani, A. M. M., Tseng, C. J., Osman, N. X-ray analyses and crystallography data of NiO–$BaCe_0$. 54Zr_0. 36Y0. 1O2. 95 composite anode for protonic ceramic fuel cell. Materials Today: Proceedings, vol 66 (2022) pp.3989-3992. https://doi.org/10.1016/j.matpr.2022.04.839

[4] Cheng, P. C., Lee, K. R., Bhavanari, M., Su, P. C., Osman, N., Lee, S. W., Tseng, C. J. Enhancing protonic ceramic fuel cell performance through nanomilling of BCZY electrolyte powder. Ceramics International, vol 49, issue 19 (2023) pp.32172-32180. https://doi.org/10.1016/j.ceramint.2023.07.188

[5] Osman, S. H., Zakaria, Z., Kamarudin, S. K., Abdullah, M. K. Catalyst modification in direct ethanol fuel cell: An update. Ionics, vol 30, issue 9 (2024) pp.5141-5158. https://doi.org/10.1007/s11581-024-05697-w
[6] Bedi, U. Recent advances in fuel cell design and modeling: A comprehensive review. Next Energy, vol 11 (2026) pp.100517. https://doi.org/10.1016/j.nxener.2026.100517
[7] Malik, L. A., Samat, A. A., Jani, A. M. M., Jamil, Z., Othman, N. H., Tseng, C. J., Osman, N. Electrode reaction routes analyses of modified Ni-BCZY anode via distribution relaxation times: 1-D interpretation. Materials Chemistry and Physics, vol 333 (2025) pp.130353. https://doi.org/10.1016/j.matchemphys.2024.130353
[8] Liu, F., Duan, C. Direct-hydrocarbon proton-conducting solid oxide fuel cells. Sustainability, vol 13, issue 9 (2021) pp.4736. https://doi.org/10.3390/su13094736
[9] Qiu, P., Sun, S., Yang, X., Chen, F., Xiong, C., Jia, L., Li, J. A review on anode on-cell catalyst reforming layer for direct methane solid oxide fuel cells. International Journal of Hydrogen Energy, vol 46, issue 49 (2021) pp.25208-25224. https://doi.org/10.1016/j.ijhydene.2021.05.040
[10] Hao, N. H., Kim, Y., Lee, K., Hwang, J., Park, J. S. High performance of direct ethanol-fueled protonic ceramic fuel cells via ethanol steam reforming using non-noble metal catalysts. Electrochimica Acta, vol 481 (2024) pp.143994. https://doi.org/10.1016/j.electacta.2024.143994
[11] Pinczes, M. P., Dhawale, D. S., Elmutasim, O., Giddey, S. Hydrogenous solid oxide fuel cells: Role and evolution of anode materials. Progress in Materials Science (2026) pp.101690. https://doi.org/10.1016/j.pmatsci.2026.101690
[12] Mazlan, N. W., Murat, M. S., Tseng, C. J., Hassan, O. H., Osman, N. Lattice expansion and crystallite size analyses of NiO-BaCe0. 54Zr0. 36Y0. 1O3-δ anode composite for proton ceramic fuel cells application. Energies, vol 15, issue 22 (2022) pp.8520. https://doi.org/10.3390/en15228520
[13] Safian, S. D., Abd Malek, N. I., Malik, L. A., Azad, A. K., Luengchavanon, M., Tseng, C. J., Osman, N. Lanthanum-ferrite based cathode: Impedance data interpretation via complex nonlinear least-squares and distribution of relaxation times analyses. Ceramics International, vol 50, issue 20 (2024) pp.40518-40525. https://doi.org/10.1016/j.ceramint.2024.05.446
[14] Yusof, N. H. B., Tseng, C. J., Yazid, H., Jani, A. M. M., Osman, N. XRD and DC conductivity studies of CeO2-BaO anode catalyst for the robust proton ceramic fuel cell applications. Solid State Science and Technology, vol 34, issue 1 (2026) pp.11-18. https://doi.org/10.66514/ssst34-1-11-18
[15] Nur Syafkeena, M. A., Osman, N., Hassan, O. H. Electrical conductivity of Y3+ doped Ba (Ce, Zr) O3 in wet N2 atmosphere prepared with the addition of Brij-97. Solid State Phenomena, vol 307 (2020) pp.160-165. https://doi.org/10.4028/www.scientific.net/SSP.307.160
[16] Lazanas, A. C., Prodromidis, M. I. Electrochemical impedance spectroscopy─ a tutorial. ACS Measurement Science Au, vol 3, issue 3 (2023) pp.162-193. https://doi.org/10.1021/acsmeasuresciau.2c00070
[17] Senari, S. M., Osman, N., Jani, A. M. M. Impedance study on NiO-BaCe0. 54Zr0. 36Y0. 1O2. 95 composite anode for proton-conducting fuel cell. Journal of Physics: Conference Series, vol 1083, issue 1 (2018) pp.012026. https://doi.org/10.1088/1742-6596/1083/1/012026
[18] Karmakar, S. Impedance spectroscopy for electroceramics and electrochemical system. arXiv preprint arXiv:2406.15467 (2024). https://doi.org/10.48550/arXiv.2406.15467
[19] Wang, X., Wang, J., Sun, Y., Li, K., Shang, T., Wan, Y. Recent advances and perspectives of CeO2-based catalysts: Electronic properties and applications for energy storage and conversion. Frontiers in Chemistry, vol 10 (2022) pp.1089708. https://doi.org/10.3389/fchem.2022.1089708
[20] Tsvetkov, N., Kim, D., Jeong, I., Kim, J. H., Ahn, S., Lee, K. T., Jung, W. Advances in materials and interface understanding in protonic ceramic fuel cells. Advanced Materials Technologies, vol 8, issue 20 (2023) pp.2201075. https://doi.org/10.1002/admt.202201075

[21] Anwar, M. F., Yu, Y., Khalid, M., Nazar, A., Bibi, B., Sarfraz, M. F., Asghar, M. I. Electrochemical insights into performance enhancement of protonic ceramic fuel cells with Ba (Zr, Ce, Y) O3-δ electrolyte. Energy Materials, vol 5, issue 8 (2025). https://doi.org/10.20517/energymater.2025.16

[22] Meisel, C., Kim, Y. D., Diercks, D., O'Hayre, R., Sullivan, N. P. Advancing proton-conducting ceramic electrochemical devices: Perspectives on benchmarking and barriers to progress. Frontiers in Energy Research, vol 13 (2025) pp.1565315. https://doi.org/10.3389/fenrg.2025.1565315

Conflict of interest statement: The authors declare that they have no known competing financial interests or personal relationships that could have appeared to influence the work reported in this paper.

Author contributions statement : Conceptualization, S.D. Safian, A.K. Azad, L.A. Malik and A.M.M. Jani; Methodology, N.H. Yusof; Validation, S.D. Safian and A.M.M. Jani; Formal Analysis, N.H. Yusof; Investigation, N.H. Yusof; Data Curation, N.H. Yusof, S.D. Safian and L.A. Malik; Writing – Original Draft Preparation, N.H. Yusof; Writing – Review & Editing, S.D. Safian, L.A. Malik, A.M.M. Jani and N. Osman; Visualization, N.H. Yusof; Supervision, S.D. Safian, L.A. Malik, A.M.M. Jani and N. Osman; Project Administration, N. Osman; Funding Acquisition, N. Osman.

Declaration of Generative AI Use: During the preparation of this work, the authors used ChatGPT, Gemini, and Scopus AI to assist with initial literature exploration, the development of the research framework, and the improvement of language, readability, and writing quality. All information, references, and generated content were critically reviewed, verified, and revised by the authors. The authors take full responsibility for the accuracy, integrity, and final intellectual content of this publication.

Data Availability Statement: Data will be made available on request.